Theor Chem Acc (2004) 112: 40–51
DOI 10.1007/s00214-003-0558-8

Theoretical
Chemistry Accounts

Regular article

An approach to reaction path branching using valley–ridge inflection points of potential-energy surfaces

Wolfgang Quapp[1], **Michael Hirsch**[1], **Dietmar Heidrich**[2]

[1] Mathematisches Institut, Universität Leipzig, Augustus-Platz, 04109 Leipzig, Germany
[2] Wilhelm-Ostwald-Institut für Physikalische und Theoretische Chemie, Universität Leipzig, Johannisallee 29, 04103 Leipzig, Germany

Received: 12 May 2003 / Accepted: 10 November 2003 / Published online: 4 March 2004
© Springer-Verlag 2004

Abstract. Valley–ridge inflection (VRI) points of a potential-energy surface (PES) may have a strong relation to the occurrence of bifurcations along reaction pathways of molecular rearrangements. We discuss two different definitions of VRI points in the literature. The calculation of symmetric VRI points has already been reported [W. Quapp et al. (1998) Theor. Chem. Acc. 100: 285–299]. Here, we in addition calculate special asymmetric VRI points which are placed on gradient extremals (GE). Following a GE opens the possibility to find the VRI point on it. An application is presented to search for asymmetric VRI points near the isomerization valley of the PES of the HCN molecule. A new method for GE-following is based on a mathematical connection between the following of a reduced gradient and the calculation of GEs. The tangent search method to follow a GE to the smallest eigenvalue [W. Quapp et al. (2000) Theor. Chem. Acc. 105: 145–155] is extended to follow also GEs to higher eigenvalues in order to find a VRI point. The new method needs gradient and second derivatives of the PES only.

Keywords: Reaction path following – Projected gradient – Gradient extremal – Valley–ridge inflection point

1 Introduction

Potential-energy-surface (PES) analysis remains an important basis for classifying and understanding the fundamentals of chemical reactions and their dynamics. It leads to the conception of the so-called minimum energy path, or the reaction path (RP) on a PES [1], which is an important theoretical tool in reaction theory with high intuitive power for chemists. The RP is roughly defined [2, 3] as the line which connects two minimizers by passing the saddle point (SF) of the PES following the valley in between. The whole chemical reaction (gross reaction) may be composed of a number of such elementary processes forming the mechanism of the reaction. The RP is conventionally defined by the mass-weighted steepest descent (SD) from the SP, the intrinsic reaction coordinate (IRC) [4, 5, 6, 7]. There are a number of other RP definitions. The curves which follow projected gradients (reduced gradient following-RGF) can be used in certain cases to characterize the reaction channel [10, 11]. Some special gradient extremals (GEs) [11, 12, 13, 14, 15, 16, 17, 18] also appeared to form a suitable ansatz for valley floor lines. Recently, Quapp et al. [19] proposed the tangent search concept (TASC) method to calculate the valley extremal using the gradient and the Hessian of the PES only. In the present paper we extend the RGF and TASC methods to follow other GEs using again first and second derivatives only. We employ certain GEs that describe the chemically interesting situation of valley or cirque structures of a PES, as well as their complements of ridges or cliffs [16, 20]. This opens the possibility to find valley–ridge inflection (VRI) points and, in succession, bifurcation or branching points (BPs) of RPs. The mathematical description of RP-branching is of great interest. In our opinion, it is one of those questions which now requires closer consideration in PES computational chemistry:

"The rate of a reaction can be estimated by transition state theory from the energy, structure, and vibrational frequencies of the transition state. Reaction path following can identify with some certainty the reactants and products connected by the transition state, unless the path branches. If the branching occurs before the transition state, there will be a separate transition state for each branch, and transition state theory can be used to estimate the relative rates. If the branching occurs after the transition state, ... , the branching ratio cannot be determined by transition state theory, but depends on the nature of the potential energy surface as it descends from the transition state toward the different products. ..." [21].

Correspondence to: W. Quapp
e-mail: quapp@rz.uni-leipzig.de

There are a number of older as well as recent studies dealing with aspects of the definition of RPs and their bifurcation: a sizable literature exists concerning BPs [15, 16, 20, 21, 22, 23, 24, 25, 26, 27, 28, 29, 30, 31, 32, 33, 34, 35, 36, 37, 38, 39, 40, 41, 42, 43, 44, 45, 46, 47, 48, 49, 50, 51, 52, 53, 54, 55, 56, 57, 58, 59, 60, 61, 62, 63, 64, 65, 66, 67, 68, 69, 70, 71, 72, 73, 74, 75, 76, 77, 78, 79, 80, 81, 82, 83, 84, 85, 86, 87, 88, 89, 90, 91, 92, 93, 94, 95, 96, 97, 98, 99, 100, 101, 102, 103, 104, 105, 106, 107, 108, 109, 110, 111, 112, 113, 114, 115, 116, 117, 118, 119, 120, 121, 122, 123]. (Papers with RP bifurcations are legion.)

Looking for the potential of the usual RP-following to locate bifurcations, we have to treat firstly the IRC [7, 8, 124, 125]. It is a simple RP concept forming the SD from an SP. This pathway is defined by an autonomous system of differential equations for a tangent vector along the curve searched for. Its solution is unique; therefore, no bifurcation can occur before reaching the next stationary point. Hence, no branching of PES valleys will be truly described by following the IRC, see the discussion in Refs.[79, 81], and Figs. 1, 2, 3 and 4.

It is helpful to consider that RP-branching is in many cases connected with the emergence of a special class of points of the PES, the VRI points [10, 26, 35]; we first give a definition of these points.

Definition 1 (traditional): A VRI point is that point in the configuration space where, orthogonally to the gradient, at least one main curvature of the PES

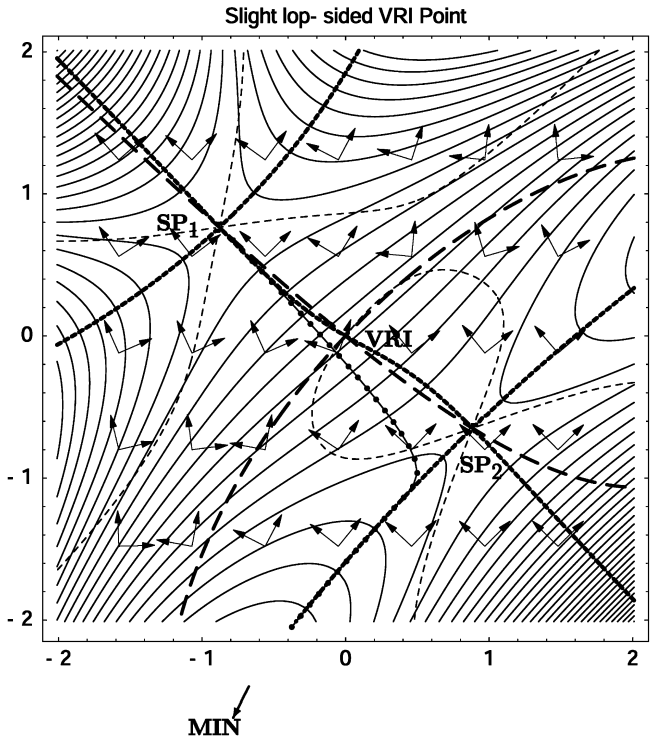

Fig. 2. Equipotential lines of 2D model PES (2) with $\mu = 1.75$. The IRC from Saddle point(SP_1) is the *dotted line*. GEs are the *thick dotted curves*, RGFs are the *bold dashes*. Pairs of eigenvectors of the Hessian are shown at a grid of points. The *thin dashed lines* are the border (3) between the valley and the ridge of the PES

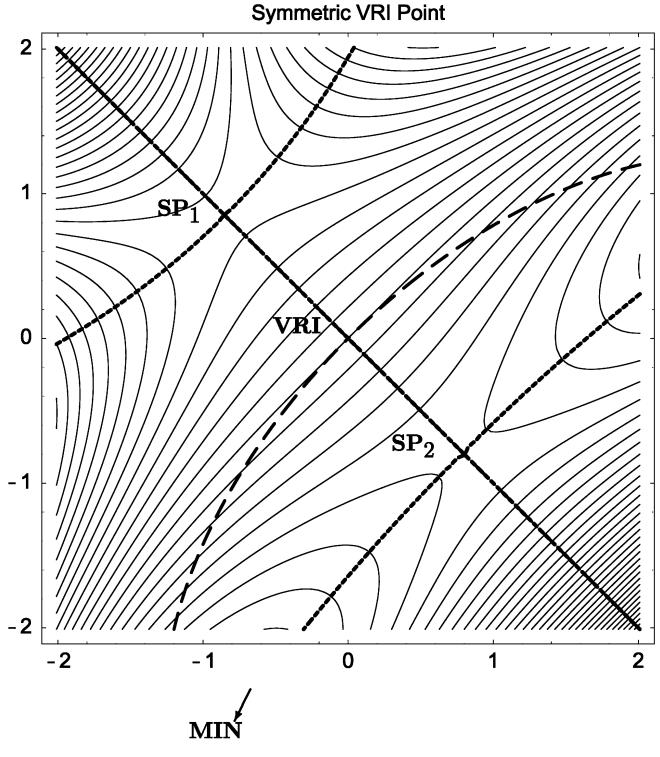

Fig. 1. Equipotential lines of a model potential-energy surface (*PES*) (2) with $\mu = 2$. Gradient extremals (*GEs*) are shown as *thick dotted curves*, reduced gradient following (*RGFs*) as *bold dashes*. (The *diagonal line* is GE, RGF, as well as the intrinsic reaction coordinate *IRC*.) The valley–ridge inflection (*VRI*) point is at (0, 0)

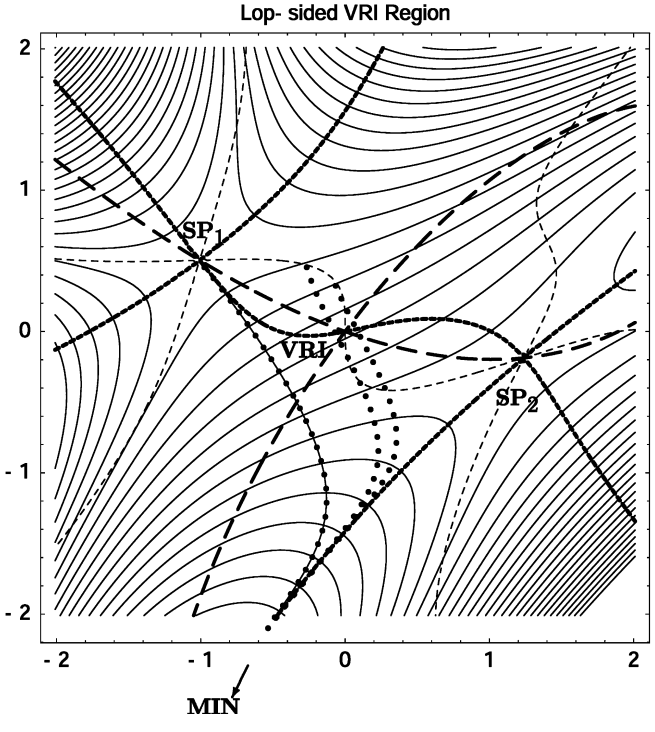

Fig. 3. Equipotential lines of model PES (2) with $\mu = 1$. The IRC from SP_1 is the *dotted line*, and two further steepest descent lines are given by *dots*. They go from valley to ridge: the *thin dashed lines* are the border (3) between the valley and the ridge of the PES

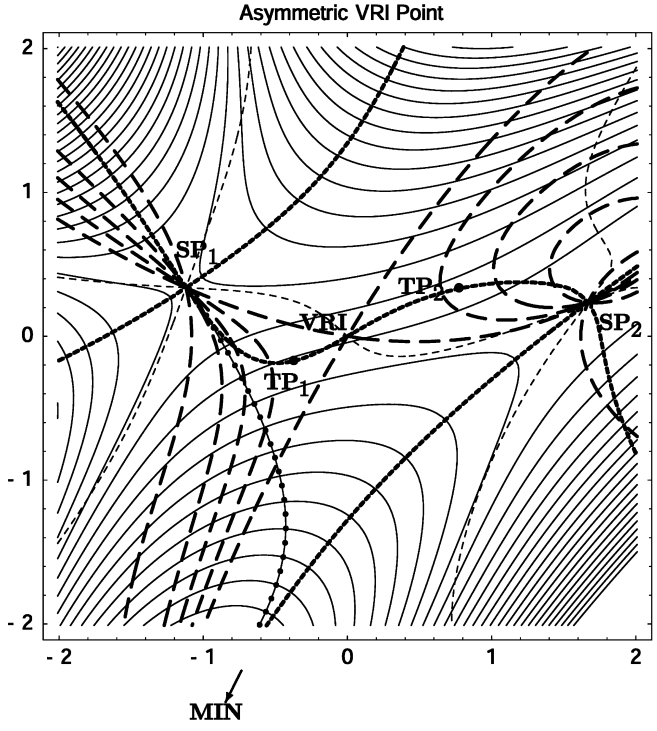

Fig. 4. Equipotential lines of model PES (2) with $\mu = 0.5$. A family of RGF curves (*bold dashes*) is additionally shown, where corresponding branches lead from SP_1 to MIN. *TPs* are turning points of the GE from SP_1 to the VRI to SP_2

becomes zero. This has two conditions: 1. one eigenvalue of the Hessian must be zero, and 2. the gradient is orthogonal to the corresponding zero eigenvector.

VRI points in the narrow sense of definition 1 are given independently of an RP definition (in contrast to the weaker definition 2, see later). VRI points are, in general, not identical with BPs of any RP. Usually, VRI points represent nonstationary points of the PES [35]. A failure of the IRC concept is that the IRC can miss asymmetric VRI points, see Figs. 2, 3 and 4.

A favorable approach to find the RP-branching is the RGF [10]. The method utilizes the fact that VRI points are the BPs of RGF curves. The RGF method finds a curve with a selected gradient direction at every curve point [9, 10, 127, 128]:

$$\mathbf{g}(\mathbf{x})/\|\mathbf{g}(\mathbf{x})\| = \mathbf{r} \ , \tag{1}$$

where $\mathbf{r}$ is the unit vector of the search direction, and $\mathbf{g}$ is the gradient of the PES. Different branches of the solution of the same reduced gradient curve with respect to $\mathbf{r}$ may cross each other. Such crosspoints of the reduced gradient curve form the VRI points of the surface [10]. Of course, not every RGF curve has such a BP. The path following along those RGF curves which have a BP allows one to find VRI points—but finding such curves is the problem.

Curves equivalent to RGF are obtained by the global Newton method (Branin curves [10, 129]). Branin's method is additionally well adapted to exactly calculate symmetric VRI points [10]. There have been successful applications to H_2O [121], H_2S, H_2Se, and H_2CO [122], and $C_2H_5^+$ [123]. However, the calculation of asymmetric VRI points on RPs is still an open task and a challenge for theoreticians. In the present paper a first solution is proposed—still for a subset of asymmetric VRI points on GEs.

GEs show an intrinsic possibility for finding a VRI point. They are defined by curves where the gradient itself is an eigenvector of the Hessian. If there is a point where another eigenvector has a zero eigenvalue, the point automatically is the VRI point. GEs are significantly more complicated than the IRC, but are well suited to help us find VRIs. In this paper, we use the GE from a stationary point as the leading line to find the next VRI point. (At least, the combination of the GE concept with RGF opens a calculable way to follow every GE of the surface.)

The first modification of the RGF method to follow a GE was TASC [19]. The constant search direction $\mathbf{r}$ for the gradient of Eq. (1) is replaced by a variable direction: the tangent of the curve searched itself. The corrector steps are calculated using the tangent direction of the previous predictor for the search direction. This quickly leads to self-consistency on the valley floor GE. (There is a convergence proof of TASC [126].)

A second modification of RGF to reach GE-following is proposed in this paper. It uses a deeper analysis of the action of TASC: its self-consistency for the direction of the first eigenvalue. This does not work for the continuation of GEs to higher eigenvalues. So, the next step is again a change of the search direction. We use the eigenvector of the GE of interest to define the projector for the gradient search. Mathematical complications connected with such an idea are discussed, and a general procedure is derived.

The paper is organized as follows. The next section gives an answer to the question: why is it not clever to search for an asymmetric, a "lopsided", VRI point using the SD from the SP. We employ a sequence of simple 2D examples. Additionally, we discuss the two different definitions of VRI points from the literature. The fundamentals of the RGF method and the definition of GEs are briefly recalled in Sects. 3 and 4. We illustrate the importance of VRI points on GEs in the 3D configuration space of the HCN molecule in Sect. 5. The TASC method is recalled briefly in Sect. 6. After that the new idea of numerically following the "higher eigenvalue" GEs is introduced: a new version of a modified RGF is proposed.

2 Why it is difficult to find a lopsided VRI point?

At the very beginning we stated that an RP connects two mimima of the PES via a transition state; however, this simple definition does not exclude more complex courses of reactions passing additional SPs between reactant and product [51]. A sample PES can be described by a valley descending from the higher-energy SP, thereby leading into another ("orthogonal") valley. If the descending valley comes from the side slope, and if there emerges a symmetric ridge in between, we find a symmetric VRI, or alternatively in the asymmetric case, a lopsided VRI

point. (Then the question emerges whether to include the VRI point and the lower SP into an RP definition, or not!) The following four examples show different situations of such sequential SPs. We treat the test function

$$E(x,y) = \frac{1}{2}(xy^2 - yx^2 - \mu x + 2y) + \frac{1}{30}(x^4 + y^4) \ , \qquad (2)$$

where μ is a parameter. We use $\mu = 2$, 1.75, 1, and 0.5 to generate a sequence of VRI points of different environments on the PES. Figure 1 starts with the symmetric case, $\mu = 2$, of the PES (2). Note that three minima of the surface exist outside the figure, where the minimum at the top left is considered as the reactant, and the two other minima represent the two products. Two SPs with orthogonal valleys are shown. An SD pathway (IRC) leads from SP_1 to SP_2. The IRC here coincides with a GE. Because of symmetry conservation the IRC leads from SP_1 to the second transition state. But the second part of the pathway, near SP_2, leads down along a ridge. The point (0, 0), where the first valley ends, and meets the ridge, is the VRI point. The VRI point can be a bifurcation point, from which RPs may lead to one of two product minima. However, the IRC does not follow the possible RP-branching. After the VRI point, the IRC as well as the GE pass the "unstable" region along the crest of the ridge [3, 33, 34, 68, 75]. An example for such a PES has already been found for the thioformaldehyde molecule, where the VRI emerges by the second-order Jahn–Teller effect [69, 70, 78]. Both IRC and GE do not reflect that there are two valleys besides the ridge leading to the two product minima. They cease to be useful definitions of the RP. Only in the case of a numerical uncertainty, the calculation of SD leaves the symmetric IRC and reaches, after a more or less long adaption, one of the valleys. If the symmetry is held, the IRC is the method of choice to calculate the VRI point: by taking a test for the zero eigenvalue belonging to an orthogonal eigenvector [38]. Note an inflection point of an energy profile along a RP is generally not a VRI point, because the gradient is not orthogonal to the corresponding zero eigenvector. A special RGF curve is included in Fig. 1. One branch of the RGF also coincides with the IRC from SP_1. At every point on this curve, the gradient of the PES has the same direction (−1, 1). The RGF curve has a bifurcation point at the VRI point and the bifurcating branches reflect the symmetry break. One may consider the RGF curve as a model of an RP. It is composed of the branch from SP_1 to the VRI and of the two pitchfork tines from the VRI to one of the two product minima correspondingly. We have the problem of a "cornered" RP model. But that is always the case under bifurcation: it does not lead to smoothly leaving branches. Nevertheless, this pathway is "shorter" than the IRC from SP_1 to a minimum via the SP_2.

A slightly disturbed symmetry of the surface (2) using $\mu = 1.75$ is shown in Fig. 2; compare it with an example in Ref. [39]. Now, the IRC leads directly from SP_1 to the left-hand deeper valley below, but the GE further follows the crest of the ridge to connect the two SPs. The VRI point is again at (0, 0) on the GE; it is not on the IRC from SP_1. Note that the IRC leaves the asymmetric ridge without any violation of a restriction: the IRC and GE follow their own ways, both are asymmetric. The IRC from SP_1 can lead only to one product [22]. A question emerges: is there a point where the SD meets a direction with zero curvature of the PES orthogonal to the gradient? The answer is yes, it happens at the two points where the IRC meets the border of the ridge region. That border is defined by

$$\mathbf{g}^{\mathrm{T}}\mathbf{A}\mathbf{g} = 0 \ , \qquad (3)$$

where **A** is the adjoint matrix [10] to the Hessian, **H**. **A** is defined as $[(-1)^{i+j}m_{ij}]^{\mathrm{T}}$, where m_{ij} is the minor of **H** obtained by deletion of the ith row and the jth column from **H**, and taking the determinant. The superscript T denotes the transposition. Equation (3) is given here for the first time. At the border, of course, a valley–ridge transition occurs. So, we may use it for a second definition.

Definition 2: A valley–ridge transition point on the IRC is the first intersection of the IRC with the manifold of solutions of Eq. (3).

There, the gradient is not orthogonal to one of the eigenvectors of the PES, in the general case, and both of the two eigenvalues are not zero. The zero curvature of the PES along the level line comes from a suitable linear combination of the two eigenvalues. The VRI point is a special point on that border, but the general points of that border do not fulfill the narrow definition 1 of the VRI point. In Fig.2 we include couples of eigenvectors of the PES, at a grid of points, to be able to compare the gradient and the eigenvectors of the Hessian. Throughout the GE, the gradient is by definition an eigenvector of the PES. And also at the VRI point on the GE, the gradient is orthogonal to the zero eigenvector. (In two dimensions then the gradient is always an eigenvector at the VRI). In contrast, this is, in general, not the case along the IRC. There does not exist a VRI point with definition 1. The IRC goes anywhere through the region of the ridge and meets definition 2. Understanding the IRC from SP_1 to be the only possible RP model then there would be no RP bifurcation at the valley–ridge transition; however, there is a valley branching at the VRI region.

We stress that the 7D-projection **(1-P)H(1-P)**, where the IRC direction is included in the **P**-matrix [38, 79, 80, 120] additionally to the six "zero" directions to translation and rotation [130], would give in the asymmetric case a valley–ridge transition definition in analogy to definition 2. It then changes the usual point of view of a VRI to a weaker perspective [131]. The aim of the projection is to find "zero" directions orthogonal to the IRC; however, these directions are not eigenvectors of the Hessian of the full surface.

The special RGF curve to the gradient direction $(-\mu, 2)$ with $\mu = 1.75$ is also included in Fig. 2. It is the curve which has a BP at the VRI point. It may serve as an RP model with bifurcation, alternatively to the IRC.

A further extension of Eq. (2) to the more asymmetric lopsided VRI case with $\mu = 1$ is shown in Fig. 3. Again, the VRI point is at (0, 0) on the GE, which again connects SP_1 and SP_2. The GE curve

carries the VRI. The IRC deviates early from this GE by going down the slope to the deeper minimum. The type of SP_1 is related to Jensen's "side-on" type SP [67, 132]. The symmetry is so strongly disturbed that the IRC does not meet the ridge region; however, there is a "remainder" of a valley–ridge transition near the VRI point. We show two SD lines (meta-IRCs [125]) which include this region (bullet lines). They come from a valley region with convex behavior of the PES and they pass or touch the ridge region with concave behavior. Finally, they asymptotically approach the deeper valley like the IRC from SP_1. Included in Fig.3 is again the border (3) between the valley and the ridge of the PES. A curve like the GE from SP_1 over the VRI to SP_2 is assumed by some workers to be not a good RP model [68] because SD lines from above intersect the GE under large crossing angles. However, a dynamically favored non-SD path from SP_1 [21, 107, 111] may directly find the second minimum at the right-hand side of Fig. 3. Thus, there is a valley branching. The special RGF curve with gradient direction $(-\mu, 2)$ with $\mu = 1$ is included in Fig. 3. It has a BP at the VRI point. It may serve as an RP model with bifurcation.

Finally, Fig. 4 refers to the case of Eq. (2) with $\mu = 0.5$. It is a further extension of the asymmetry of the PES. The qualitative description is equal to that of Fig. 3. However, the GE between the downward valley of SP_1 and the uphill crest of SP_2 shows two turning points (TPs). So, the structure of the GE becomes more complicated [14, 15]. TP_1 marks the end of the valley of SP_1, whereas TP_2 marks the end of the ridge of SP_2. The VRI point is only a point of the border between the ridge above and the valley below. But also in this case there is the VRI point (0, 0) on the GE. We conclude that there is a border between the SD valley through SP_1 and the steepest ascent ridge through SP_2. If we know the SP_1 and SP_2, as well as the VRI point in between, we may derive branching ratios of reaction trajectories [21]. The intermediate GE between the two TPs is not a model of an RP. It is a tool to calculate the VRI point. On the other hand, TP_1 forms a qualitative valley characterization: the pass valley ends here. The SD, as well as a family of RGF curves through SP_1, estimate the reaction channel to the minimum below. This family of RGF curves is bounded by the special RGF curve to the constant gradient search direction $(-\mu, 2)$ with $\mu = 0.5$. It is the curve which has a BP at the VRI point. It may again serve as an RP model with bifurcation.

The IRC from SP_1 in Figs. 2, 3 and 4 does not find the VRI point (in the narrow definition 1); however, there is in every case a special RGF curve which leads to the VRI point and bifurcates there. This curve could be obtained by trial and error (using an iteration method, in the 2D case); however, in more than two dimensions, there is no straightforward method to find the special RGF curve which bifurcates at a lopsided VRI point. The only direct way is to follow the GE. A strategy to follow a GE has already been given by Sun and Ruedenberg [17] (see also the test report in Ref. [133]); but the method needs some third derivatives of the PES. This will be avoided in the procedure proposed next.

3 Following the projected gradient (RGF)

We repeat the way to look for the RGF lines [9, 10, 121, 122, 127]: we choose a search direction $\mathbf{r}$, a unit vector, and define a projector $\mathbf{P_r}$ which realizes $\mathbf{P_r r} = \mathbf{0}$. It is a constant matrix of rank $(n-1)$. If there is a point $\mathbf{x}$ where the gradient $\mathbf{g}(\mathbf{x})$ fulfills the system of projector equations

$$\mathbf{P_r g}(\mathbf{x}) = \mathbf{0} \tag{4}$$

then this gradient is named the reduced gradient with respect to the direction $\mathbf{r}$. Solutions of Eq. (4) build the RGF curve to direction $\mathbf{r}$. It connects stationary points which differ in their index by 1, if no BP is crossed. We numerically follow the curve (4) by tangent continuation. The tangent $\mathbf{x}'(t)$ is obtained by the solution of the system of the derivative to the curve parameter:

$$\mathbf{0} = \frac{\mathrm{d}}{\mathrm{d}t}\{\mathbf{P_r g}[\mathbf{x}(t)]\} = \mathbf{P_r}\frac{\mathrm{d}\mathbf{g}[\mathbf{x}(t)]}{\mathrm{d}t} = \mathbf{P_r H}[\mathbf{x}(t)]\mathbf{x}'(t) \ . \tag{5}$$

In general, the search direction, $\mathbf{r}$, and the tangent, $\mathbf{x}'(t)$, to the RGF curve with respect to $\mathbf{r}$ are different. The predictor–corrector method of RGF is the predictor step along the tangent $\mathbf{x}'(t)$ and Newton–Raphson steps of the corrector to search (usually orthogonal to this direction) a solution of curve (4) [9, 10, 19, 127, 128, 134]. The simplicity of RGF is based on the constancy of the $\mathbf{P_r}$ matrix which is used in Eq. (5). We recall that RGF curves are not generally the so-called valley ground pathways, or valley floor lines. Nevertheless, these curves may follow a valley in favorable cases, at least qualitatively. Like SD curves, RGF curves also form a dense family of curves in the coordinate space. If $\mathbf{g}(\mathbf{x}) \neq \mathbf{0}$ then the point $\mathbf{x}$ is the carrier of an RGF curve with respect to $\mathbf{r}$, where $\mathbf{r} = \mathbf{g}(\mathbf{x})/\|\mathbf{g}(\mathbf{x})\|$.

4 Gradient Extremal

4.1 Definition of GE

$\mathbf{g}(\mathbf{x}) \neq \mathbf{0}$, and we assume we are on a "valley ground" of the PES. A point showing the gentlest ascent of the valley is defined by the condition that the norm of the gradient forms a minimum taken along an equi-subsurface, $E(\mathbf{x}) = c$, where c is constant, i.e. in all directions perpendicular to the gradient [11, 12, 14, 16]. The measure for the ascent of the PES, $E(\mathbf{x})$, is the norm of the gradient vector, the functional

$$\sigma(\mathbf{x}) := \frac{1}{2}\|\mathbf{g}(\mathbf{x})\|^2 \ . \tag{6}$$

We treat the problem to minimize $\sigma(\mathbf{x})$ where the nonlinear constraint is $E(\mathbf{x}) = c$. Thus, the function to optimize and the constraint are developed from the PES itself.

It results in the basic eigenvector relation

$$\mathbf{H}(\mathbf{x})\ \mathbf{g}(\mathbf{x}) = \lambda(\mathbf{x})\mathbf{g}(\mathbf{x}) \ . \tag{7}$$

The proportional factor $\lambda(\mathbf{x})$ is an eigenvalue of the Hessian matrix, and the gradient is its eigenvector. Curves $\mathbf{x}(c)$ defined by Eq. (7) consisting of such points

on consecutive equi-hypersurfaces for different sections of increasing or decreasing c are termed GEs [14]. If $\sigma(\mathbf{x})$ has a minimum, the PES usually has a valley extremal, however, it may also have a crest of a ridge.

4.2 Relation between GE and SD

With arc length s for the curve parameter, an SD curve $\mathbf{x}(s)$ and its curvature vector are defined by

$$\frac{\mathrm{d}\mathbf{x}(s)}{\mathrm{d}s} = -\frac{\mathbf{g}(\mathbf{x}(s))}{\|\mathbf{g}(\mathbf{x}(s))\|}, \quad \mathbf{k} = \frac{\mathrm{d}^2\mathbf{x}}{\mathrm{d}s^2} \ . \tag{8}$$

One finds the following relation: GEs consist of points where SD lines have zero curvature [17, 135].

4.3 Relation between GE and RGF

A point $\mathbf{x}$ belongs to a GE if the tangent of an RGF curve through this point is parallel to the gradient [126]. The proof is easy. If $\mathbf{e}_1, \ldots, \mathbf{e}_n$ are the eigenvectors of $\mathbf{H}$ with eigenvalues $\lambda_1, \ldots, \lambda_n$ then they are also the eigenvectors of the adjoint matrix, $\mathbf{A}$, but with the eigenvalues $\mu_i = \prod_{j \neq i} \lambda_j$ [19]. The gradient is an eigenvector of $\mathbf{H}$ and also of $\mathbf{A}$ on a GE. RGFs are also solutions of the differential equation of Branin [129] by

$$\frac{\mathrm{d}\mathbf{x}}{\mathrm{d}t} = \mathbf{x}'(t) = \pm\mathbf{A}[\mathbf{x}(t)]\ \mathbf{g}[\mathbf{x}(t)] \ . \tag{9}$$

This gives the proof.

4.4 Relation between GE and VRI

The definition of a GE is that the gradient is itself an eigenvector of the Hessian. It is clear by definition 1 that if another eigenvector becomes a zero eigenvector, the point of the GE where this happens is a VRI point. Walking along a GE from a convex to a concave region, where an orthogonal eigenvalue has to change its sign, must lead to a VRI point. If one starts at a stationary point and follows a GE, it may lead to the next stationary point without change of convexity of the level hypersurfaces. However, if the GE leaves the region of convex level lines of the PES, it has to meet directly the VRI point, or it meets the VRI point "indirectly" after a TP.

Vice versa, if a GE intersects the convexity border (3) then it meets a VRI point. There the gradient is an eigenvector of $\mathbf{H}$ with eigenvalue λ_1, and the gradient is also an eigenvector of $\mathbf{A}$ with eigenvalue $\mu = \prod_{j=2}^{n} \lambda_j = 0$. To fulfill Eq. (3), one of the λ_j, $j = 2, \ldots, n$ has to be zero, the corresponding eigenvector orthogonal to the gradient is the zero eigenvector.

To take the well-known Müller–Brown (MB) potential [137] as an example in Fig. 5, there are four VRI points which all fulfill the pattern to lie on GEs. The MB potential additionally shows that our idea of VRI may be questionable, in that strong asymmetric case. VRI_1 indicates a region where a ridge uphill ends and changes into a valley. However, even in this quasi-symmetric

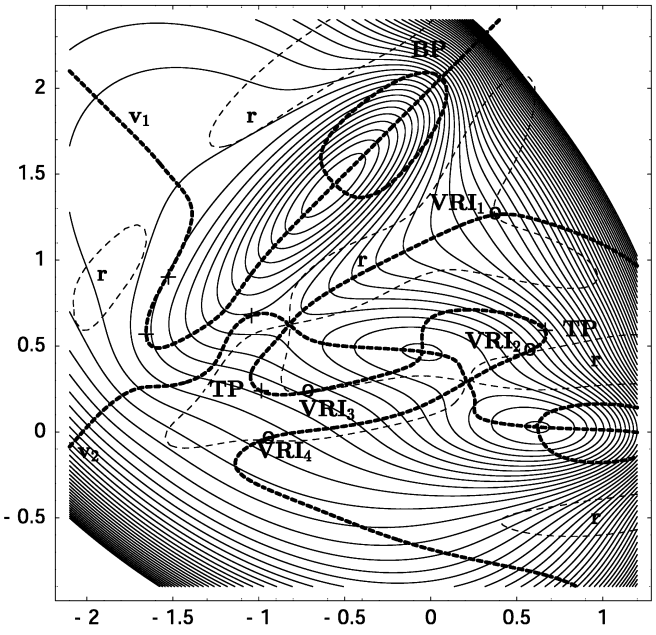

Fig. 5. The four VRI points (o) of the Müller–Brown potential lie on GEs (*bold dashes*). TPs (+) of the GE. *BP* is a branching point of a GE. The *dotted line* is the border between valleys (*v*) and ridges (*r*) of the surface

case, the two "wings" of the ridge region end uphill without a VRI point. The points VRI_2, VRI_3, and VRI_4 are located anywhere at the border of the valley–ridge coincidence, but not at extreme functional values of the ridge regions (r).

On the high-dimensional PES of a molecule, the situation is still more complex. There are more VRI points than the GE-following will find [10]. This is due to definition 1, which does not demand that the gradient is itself an eigenvector of the Hessian. It is enough if the gradient is only orthogonal to the zero eigenvector. That looseness means that, in more than two dimensions, manifolds of VRI points may exist where most of the points may not belong to a GE. It was demonstrated by calculation for three-to seven-atom molecules [121, 122, 123]. The situation for molecules is, nevertheless, not hopeless because, the valley floor GE describes with some certainty the minimum energy path of chemistry (whatever this means). If there is a VRI point on the GE, that point is in a certain sense a special minimal VRI point of the VRI manifold and it is important to calculate the special VRI points on the GEs [10].

Note that the BPs of the GE [11, 12, 13, 14, 15, 16, 17, 19, 37] are usually not the VRI points of the PES. In Fig. 5 approximately at (0.2, 2.1) there is a BP which is far away from the VRI, and the VRI points do not indicate a bifurcation of the GEs. Only TPs of the GEs indicate the beginning or the end of valleys and ridges in the asymmetric case of this test potential.

5 Application

We refer to the calculations [13] of the isomerization valley of the HCN 6-31G* potential surface:

HCN→[SP]→CNH. In this paper we extend the investigation to leave the isomerization valley at the SP by going uphill along some marked side slopes. The process of leaving the valley can only be followed within the scope of the Hartree–Fock method if dissociation is excluded. In spite of this fact we extend the PES calculations to larger distances to test the methods for BP calculation. So, we use the HCN 6-31G* PES as a model PES to develop further the tools of general RP analysis. The GEs around the nonlinear SP structure of the isomerization are shown in Figs. 6 and 7. The SP is at (CN, CH, α) = (1.169Å, 1.155Å, 77.49°). The configuration space of any nonlinear HCN is 3D and can be fully illustrated by the internal coordinates r_1, the CN distance, r_2, the CH distance, and α, the bending angle of HCN ($\alpha = 180°$ at the HCN minimum). The PES is also 3D, a hypersurface in four dimensions over the configuration space: it is not fully illustrable. (Thus, no energy is directly involved in Figs. 6, 7 and 8). The valley GE of the isomerization reaction is number 1 between HCN and the SP, and number 2 between the SP and CNH in Fig.7. The GE has an inflection point (IP) at every side of the SP where the convexity of the PES around the minima changes into the 1D concavity of the colway of the SP.

Orthogonal to the SP valley are two other eigenvectors with two positive eigenvalues. They point in the direction of the CN stretch (GEs 3, 4) and the CH stretch (GEs 5, 7). These GEs go uphill on the 3D PES along the two different normal mode directions where the bending ridge is orthogonal in both cases.

GE3 corresponds to the CN stretch. It leads to an asymmetric VRI point (1.47Å, 1.125Å, 86.3°). The VRI structure is a triangular structure like the SP. We may assume that there the dissociation channel of the N atom starts from the C–H diatom. This channel is a valley going further uphill. The N atom escapes "in front" of the diatomic CH part. Vice versa, at the corresponding VRI point, the incoming N atom has the possibility to descend to the SP or to bypass the SP to reach the HCN side of the PES. It is enlarged in Fig. 8, which includes the RGF curve through the VRI point. Additionally, in another representation Fig. 9, we have included level lines of a PES section with a fixed CH distance of 1.125Å through the VRI point. The situation is also shown schemetically in Fig. 10b. Whereas GE3 follows the ridge to the SP, the corresponding "reaction" pathway to the basin shaped valley of HCN must be calculated by means of an RGF curve (depicted by b), or by an SD (not shown). The calculation of a bifurcating RGF is quite easy if the VRI

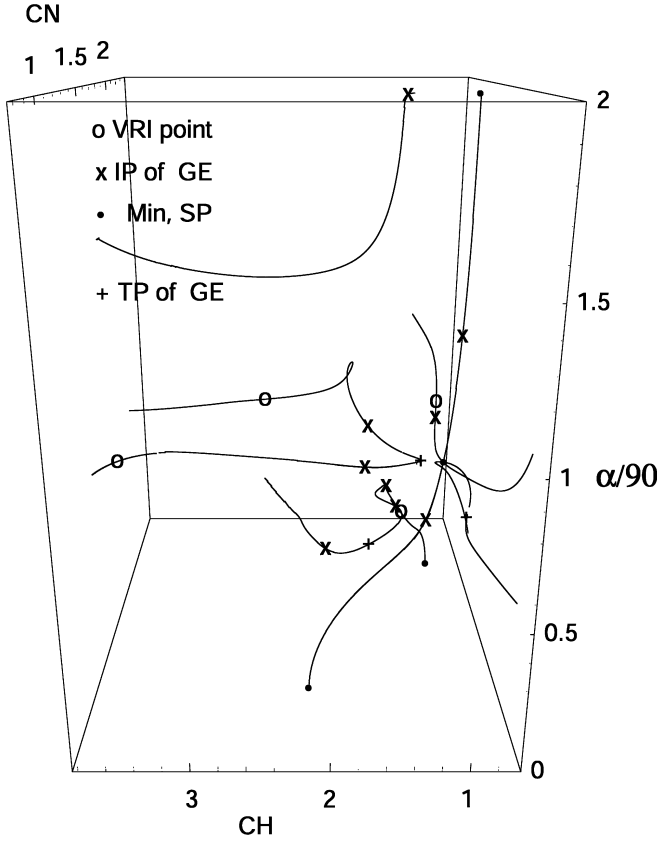

Fig. 6. GEs of the HCN 6-31G* PES in nonlinear nuclear configurations. The vertical axis is the HCN bending scaled to $\alpha/90°$, the *top* of the figure contains the HCN minimum, and the bottom the HNC minimum. Additionally, the *bottom* contains a hypothetical linear C–H–N structure which is a high–energy SP. The other two axes are the CH and the CN distance (angstroms)

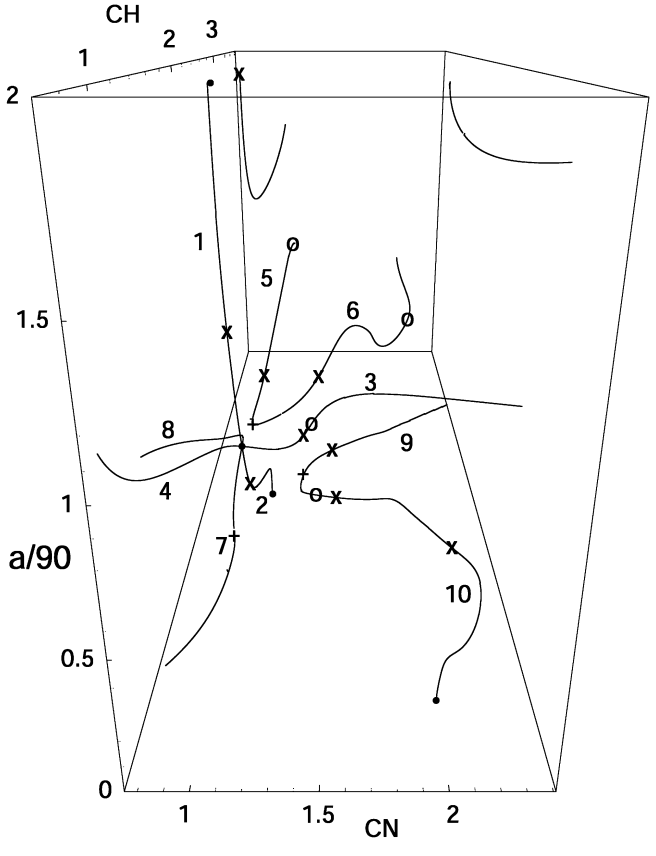

Fig. 7. GEs of the HCN 6-31G* PES in nonlinear configurations in a complementary view to Fig.6. The vertical *axis* again is the HCN bending. The other two axes are the CN distance in the foreground, and the CH distance (angstroms). The *numbers* describe individual GEs, see text

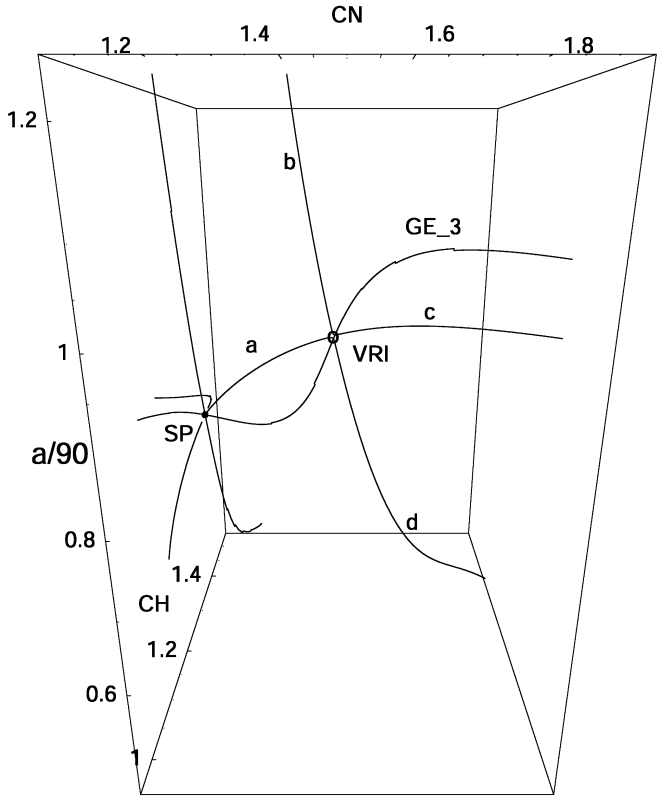

Fig. 8. Approximation of a bifurcating RGF curve of the HCN 6-31G* PES using a view like that in Fig.7. The BP is the VRI point on GE3 of Fig. 7. Branches of the RGF curve: **a**. branch between the VRI and the SP of the isomerization path; **b**. branch between the VRI and the HCN minimum; **c**. branch between the VRI and the dissociation of the single N atom; and **d**. branch between the VRI and the path to a linear SP of type C–H–N. **c** and **a** correspond to GE3. Branches **b** and **d** do not correspond to GEs. The energy increases along **c** and **d**, but decreases along **a** and **b**

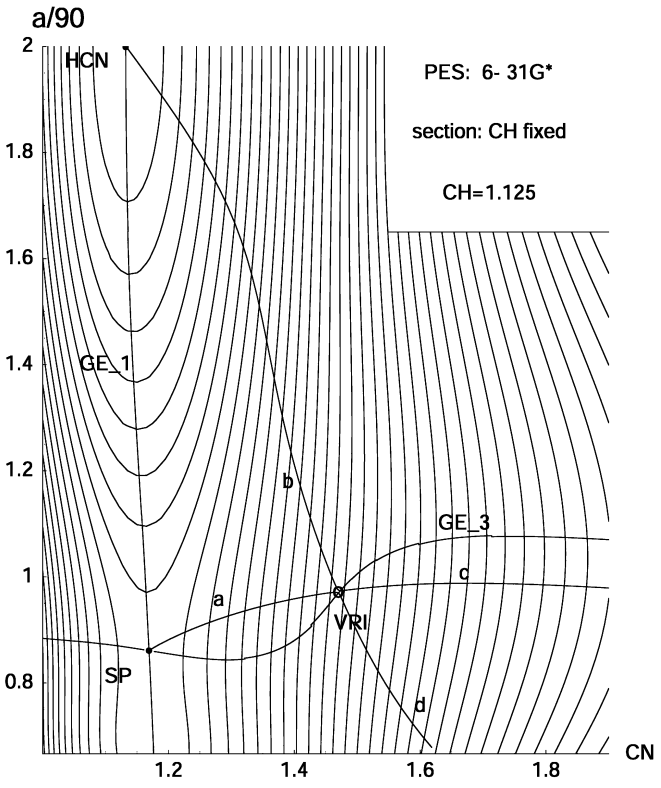

Fig. 9. 2D contour diagram of the HCN PES section for CH = 1.125 Å fixed (distance of the configuration of the VRI point). The reaction path (RP) model curves of Fig. 8 are included by the projection into the plane of the PES section. The symbols used are these of Figs. 6, 7 and 8. In the full 3D space, the CH distance varies from 1.058 Å at the minimum to 1.155 Å at the SP. The projection does not very much disturb the picture, it gives a realistic impression of the region of the VRI point, and also of the SP and minimum

point is found before on the GE. The section plane of Fig. 9 perfectly forms the tangential plane to the four branches of the RGF curve which meet the VRI point. The pattern of the RGF branches around this VRI point is comparable with Fig. 3; however, it does not include a connection of branch d to the second minimum, HNC. By the way, this VRI is not the usual "pitchfork" bifurcation, however, here an incoming valley c and a ridge d go over into an outgoing ridge a and a skew valley pathway b. The combined pathways c and b form a continuous valley for the incoming N atom, which takes a short-cut before the ridge region of the SP. Branches c and b may serve for a RP model.

Going back to Figs. 6 and 7, the alternative GE4 describes the shortening of the CN bond. It leads along a ridge to unfavorable high energies; the calculation is stopped at "chemically forbidden" energy. A GE orthogonal to GE4, as well as to the SP-col, is GE7, which describes the shortening of the CH bond. It also quickly leads to very high energies, where the calculation ends.

From the SP, the CH stretch mode is followed by GE8. This GE only leads a small distance along the ridge of the stretch followed by a sharp bend. The GE turns off and follows the CN shortening. At the other side of the kink, the "true" CH stretch is followed by GE5 up the ridge to point (1.19Å, 3.57Å, 76.7°) which is the asymmetric VRI point of the dissociation channel of the H atom from the diatomic remainder, CN. This channel forms a valley uphill. It is shown schemetically in Fig. 10a. More distant, the H atom feels the attraction of the CN group as a whole. Vice versa, at the VRI point, the incoming H atom has the possibility to turn to the CNH side of the PES, or to the SP. Whereas GE5 follows the ridge to the TP downhill, the corresponding "reaction" pathways to the minimum have to be calculated with the help of RGF, or an SD. A branch of the RGF also follows a pathway to the SP nearly parallel to GE5. The calculation of a bifurcating RGF is quite easy if the VRI point is found before on the GE.

Because of the more complicated situation owing to the existence of a TP at the lower end of GE5, there has to exist an outgoing GE (numbered 6 in Fig. 7). GE6 is at the very beginning a ridge, and it finally leads into mountains of high energy.

GEs9 and 10 fall out of the pattern of the other ridge GEs. They are shown schemetically in Fig. 10c. Whereas

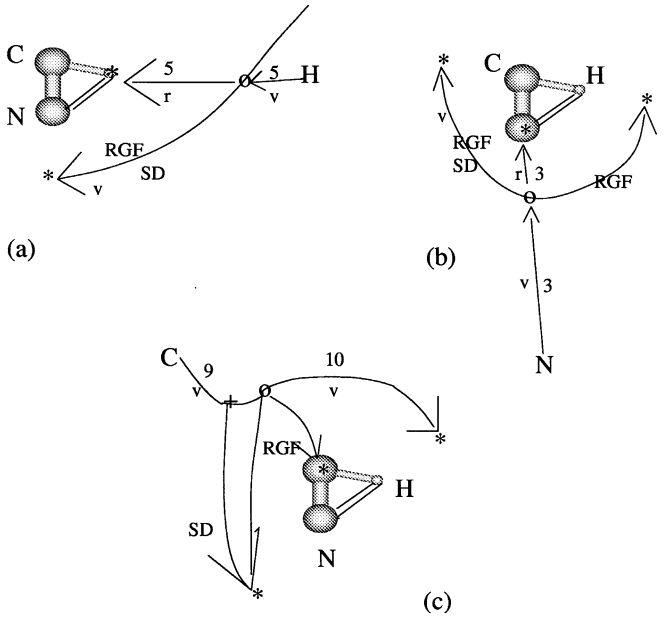

Fig. 10. Nonlinear attack of **a** the H atom, **b** the N atom, and **c** the C atom to the diatomic remainder of the (HCN molecule) followed by GE or other RP. A star is a possible stationary molecular structure of the incoming atom. The structure shown is the SP of the H isomerization path. The outer pathway of the attack is in every case a minimum pathway with a quasi T-shaped configuration. The numbering is analogous to Fig. 7. *Arrows without numbers* do not follow GEs but follow other RP models. VRI points (o) emerge where the valley (*v*) of the incoming atom changes into a ridge (*r*), whereas in **c** the valley ends anywhere at the slope of the PES at a TP (+). Steepest descent leads to the minimum connected with the VRI. Only an RGF curve connects GEs9 and 10 with the SP of isomerization. **b** is shown in detail in Fig. 8

GE9 is the dissociation channel of the C atom in an angle region between the SP and the CNH basin-shaped valley, it does not meet the isomerization SP. The lowest point of the PES along GE9 is a TP where the valley of GE9 simply ends. (Here, the GE is not a good model for an RP.) The TP situation is comparable to the TP below an SP on the MB potential of Fig. 5. An SD can start at the TP of GE9 at (1.39Å, 1.64Å, 39.47°). It leads immediately to GE2 and along this GE to the CNH minimum (not shown). GE9 continues after the TP, now described by GE10. There is a VRI point where a ridge emerges, however, going strongly uphill over two further IPs; the pathway changes at least into a valley GE leading to a further SP of index 1 with the (hypothetical) linear structure C–H–N.

As already stated, at every VRI point there is a bifurcating RGF curve. This is explicitly shown in Figs. 8 and 9. If the VRI point is found by following the GE, we start the RGF calculation at this point, and we immediately obtain the corresponding branches. If the single RGF branches are going along a convex valley they may serve as an RP model. It should be remarked that only some branches (a, c) correspond to GE curves. The combination of GEs, RGFs, and SD may give a satisfactory idea of the corresponding PES region around the VRI points.

6 Following the tangent of the previous predictor step [19]

The tangent direction of the previous curve point, from Eq. (5), iteratively becomes the search direction used in the projector. The procedure is named the TASC. But the calculations of the predictor–corrector method were still done by Eqs. (4) and (5). We define the TASC step:

1. At a point $\mathbf{x}_k$, with $\mathbf{g}(\mathbf{x}_k)/||\mathbf{g}(\mathbf{x}_k)|| = \mathbf{r}_k$ being the RGF search direction, solve

$$\mathbf{P}_{\mathbf{r}k}\mathbf{H}(\mathbf{x}_k)\mathbf{x}'_k = \mathbf{0} \tag{10}$$

to get the tangent direction $\mathbf{t}(\mathbf{x}_k) = \mathbf{x}'_k/\|\mathbf{x}'_k\|$ for the predictor step to an RGF curve with respect to $\mathbf{r}_k$, and do the step to $\mathbf{x}_k \pm s\mathbf{t}(\mathbf{x}_k)$. s is a step length.

2. Change the search direction to $\mathbf{r}_{k+1} = \mathbf{t}(\mathbf{x}_k)$ and compute $\mathbf{P}_{\mathbf{r}k+1}$ to solve the modified equation

$$\mathbf{P}_{\mathbf{r}k+1}\mathbf{g}(\mathbf{x}) = \mathbf{0} \tag{11}$$

[instead of $\mathbf{P}_{\mathbf{r}k}\mathbf{g}(\mathbf{x}) = \mathbf{0}$] by Newton–Raphson steps $\Delta\mathbf{x}^i$

$$\begin{aligned} &\left[\mathbf{P}_{\mathbf{r}k+1}\mathbf{H}(\mathbf{x}^i)\right]\Delta\mathbf{x}^i = -\mathbf{P}_{\mathbf{r}k+1}\mathbf{g}(\mathbf{x}^i), \\ &\mathbf{x}^{i+1} = \mathbf{x}^i + \Delta\mathbf{x}^i,\ i = 0, 1, \ldots,\ \mathbf{x}^0 = \mathbf{x}_k\ . \end{aligned} \tag{12}$$

If Eq. (11) is approximately fulfilled then use the solution as the new point $\mathbf{x}_{k+1}$. The point is situated on an RGF curve with respect to direction $\mathbf{r}_{k+1}$. The key idea is that like in the derivation of Eq. (5) we have also assumed a "constant" $\mathbf{P}_{\mathbf{x}'(\mathbf{t})}$ matrix in the current step. This is here an approximation, but it works self-consistently. The numerical procedure leads to the valley GE. A convergence proof of TASC was given recently [126]. The approximation of a constant $\mathbf{P}_{\mathbf{x}'(\mathbf{t})}$ matrix allows us to avoid third derivatives of the PES [19].

7 Approximate search for GEs to higher eigenvalues

7.1 Method to follow for any GE

The TASC method (implicitly) uses the property of the valley floor: the GE of the floor and a swath of RGF curves along the valley are nearly parallel. TASC calculates the floor GE by using an RGF curve to tangent direction **t**. For higher GEs, or for the GE of a finishing valley, that property does not generally hold. RGF curves may intersect the GE at a higher eigenvalue under a large angle. We circumvent that, but we further use the RGF idea. On the GE, the gradient **g** is an eigenvector $\mathbf{e}_i$ of the Hessian. We search for a curve point where

$$\mathbf{P}_{\mathbf{e}i}\ \mathbf{g}(\mathbf{x})\ = \mathbf{0}\ . \tag{13}$$

The equation is trivially fulfilled on the GE, and it is used for the corrector step. After the prediction of a point near the GE, we start with the $\mathbf{e}_i$ of that point and use the corrector for Eq. (13) to get point $\mathbf{x}_1$. Next we iteratively have to calculate the $\mathbf{e}_i$ at a solution point $\mathbf{x}_k$, $k = 1, 2, \ldots$ and repeat the corrector for Eq. (13) up to convergence. Locally, at points near the GE, the method works. (The exceptional case of a GE turning point is

given in Sect. 7.3.) The analogy of Eq. (13) to the GE Eq. (7), $(\mathbf{H} - \lambda\mathbf{I})\mathbf{g} = 0$, was already used by Jørgensen et al. [137]; however, these authors used an Equation like Eq. (12) for an approximation of the predictor step. We use it (quasi without approximation) for corrector steps back to the GE.

However, the tangent of an RGF curve to the eigenvector $\mathbf{e}_i$ cannot be used to get the predictor step. A way out is a very simple predictor step using the secant step of the two previous points, $\mathbf{x}_k$ and $\mathbf{x}_{k-1}$, of the GE:

$$\mathbf{d} = \mathbf{x}_k - \mathbf{x}_{k-1}, \text{ and } \mathbf{x}_{k+1} = \mathbf{x}_k + \mathbf{d} \ . \tag{14}$$

The method is very cheap and works well. Note that one does not economize derivations of the gradient, because in order to solve Eq. (13) by the Newton–Raphson method we again need second derivatives, or updates of the Hessian, like in RGF/TASC.

It is possible that along a GE the numbering of the eigenvalues may be changed. If one starts with a gradient equal to $\mathbf{e}_i$ near the stationary point, the λ_i may become degenerate at an $\mathbf{x}_k$ and the eigenvector $\mathbf{e}$ may assort to λ_{i-1} or to λ_{i+1} after $\mathbf{x}_k$. It is only a bookkeeping problem. But if at $\mathbf{x}_k$ the eigenvalues are exactly degenerate then the case is problematic: the eigenvectors can rotate in a plane. Following a GE it is possible to jump across such a point, for instance, by using a 2 $\mathbf{d}$ step in Eq. (14).

7.2 Search for VRI points

To solve Eq. (13) we use the Newton–Raphson method orthogonally to the search direction, which is a gradient and an eigenvector of $\mathbf{H}$. Here we observe the intrinsic difficulty of the method: near the VRI point the Newton–Raphson method has to work along a zero direction, for example, following a 1D flat potential curve orthogonal to the gradient. The Newton–Raphson method breaks down when searching on the 'flat' region. So, we are unable to determine explicitly the VRI point by this method.

The search along a GE by the generalized RGF, (Eq. 13), works before reaching (or after leaving) the VRI point. A possible VRI point has to be tested by looking for the development of the smallest (absolute) eigenvalue of all eigenvectors. If the steplength of the predictor is sufficient the VRI point may be overcome; however, if the point is nearly met, the Newton–Raphson method results in steps that are too large. Here, a further general trick works: the step length of the corrector step is restricted. It has to be smaller than the predictor step.

7.3 TPs of the GE

Another mathematical drawback of a generalized RGF-following for GEs is the emergence of GE TP. There, the gradient of the PES is orthogonal to the tangent of the GE, and the direction of the tangent changes from uphill to downhill, or vice versa (Figs. 4, 5). One can try to handle the TP by testing the angle of gradient and "tangent" direction $\mathbf{d}$ of Eq. (14). If the curve following is near a TP, one may jump across the region and, additionally, one has to change the search direction from uphill to downhill, or vice versa.

8 Conclusions and perspectives

The IRC is the most used model of the RP. This is due to the following properties:

1. Simplicity.
2. Computational economy.
3. Reproducibility.
4. Conceptually free of error.

The simplicity of the IRC is evident. For point 2, there are sometimes convergence problems near the minimum on a flat valley floor, because the IRC shows an affinity to zigzag [8], and point 3 needs a careful definition of the coordinate system [7]. (We again report the possible independence from the coordinate system for curves and VRI points in Ref.[119]. This means that we will find a VRI point no matter what coordinate system we use.) If there is a continuous valley from the SP to the minimum (convex isopotential hypersurfaces with respect to the minimum) the IRC may best serve as an RP model. However, in case of the existence of concave VRI regions along the IRC progress, point 4 is generally not fulfilled. One has to look for other RP models or modifications which may bifurcate at the VRI point.

The new model should include the RGF approach (cf. the RP Hamiltonian on RGF curves [138]) as well as the valley extremals, special GEs. Starting at a stationary point, one can follow the GE in a valley or cirque direction and search for the next VRI point at the end of the valley. Beginning at this point (using the gradient at this point for the search direction), one can calculate the branches of the corresponding RGF curve and can assign the RP model to the branches which show the "good" direction. Because there is now the possibility to calculate also asymmetric VRIs, we hope that the future will bring a broad practical significance of such points. RGF fulfills points 1–3, see [10]; however, the numeric GE calculation does not fit point 2, [17, 20]. Therefore, we propose to calculate the pathways along any GE more simply. The proposed method is a further modification of the TASC method, which is itself a modification of RGF [19]. It follows the line of the chosen GE of a PES, downhill or uphill. It uses the evaluation of the gradient and the Hessian matrix for each iteration step. The procedure is a new method for studying the GEs of a multidimensional hypersurface. It is possible that a GE starting from a stationary point can lead to a VRI point. Thus, path-following along GEs may be the tool to find VRI points (in the narrow sense of definition 1). The method is implemented as a separate FORTRAN shell. It will be distributed on request.

Acknowledgements. The work was made possible through the financial support of the Deutsche Forschungsgemeinschaft. We thank P. Caramella (Pavia) for the (last) impulse to this paper. Thanks are due to the referees for criticisms of an earlier version.

References

1. Laidler K (1969) Theory of reaction rates, McGraw-Hill, New York
2. Mezey PG (1995) In: Heidrich D (ed) The reaction path in chemistry: current approaches and perspectives. Kluwer, Dordrecht, pp 11–38
3. Mezey PG (1987) Potential energy hypersurfaces, Elsevier, Amsterdam
4. (a) Marcus RA (1966) J Chem Phys 45: 4493–4499; (b) Marcus RA (1966) J Chem Phys 4500–4504, (c) Marcus RA (1966) J Chem Phys 49: 2610–2616, (d) Marcus RA (1966) J Chem Phys 2617–2631
5. Truhlar DG, Kuppermann AJ (1971) J Am Chem Soc 93: 1840–1851
6. Fukui K (1974) J Phys Chem 74: 4161–4163
7. Quapp W, Heidrich D (1984) Theor Chim Acta 66: 245–260
8. Garrett BL, Redmon MJ, Steckler R, Truhlar DG, Baldridge KK, Bartol D, Schmidt MV, Gordon MS (1988) J Phys Chem 92: 1476–1488
9. Quapp W, Hirsch M, Imig O, Heidrich D (1998) J Comput Chem 19: 1087–1100
10. Quapp W, Hirsch M, Heidrich D (1998) Theor Chem Acc 100: 285–299
11. Basilevsky MV, Shamov AG (1981) Chem Phys 60: 347–358
12. Basilevsky MV (1981) Chem Phys 60: 337–346
13. Heidrich D, Kliesch W, Quapp W (1991) Properties of chemically interesting potential energy surfaces. Lecture notes in chemistry 56. Springer, Berlin Heidelberg New York
14. Hoffman DK, Nord RS, Ruedenberg K (1986) Theor Chim Acta 69: 265–280
15. Quapp W (1989) Theor Chim Acta 75: 447–460
16. Quapp W, Imig O, Heidrich D (1995) In: Heidrich D (ed). The reaction path in chemistry: current approaches and perspectives. Kluwer, Dordrecht, pp 137–160
17. Sun J-Q, Ruedenberg K (1993) J Chem Phys 98: 9707–9714
18. Rico JF, Aguado A, Paniagua M (1996) J Mol Struct (THEOCHEM), 371: 85–90
19. Quapp W, Hirsch M, Heidrich D (2000) Theor Chem Acc 105: 145–155
20. Ruedenberg K, Sun J-Q (1994) J Chem Phys 100: 5836–5848
21. Bakken V, Danovich D, Shaik S, Schlegel HB (2001) J Am Chem Soc 123: 130–134
22. Murrell JN, Laidler KJ (1968) Trans Faraday Soc 64: 371–377
23. Salem L, Durup J, Bergeron G, Cazes D, Chapuisat X, Kagan H (1970) J Am Chem Soc 92: 4472–4474
24. Harms SH, Wyatt RE (1972) J Chem Phys 57: 2722–2727
25. McIver JW, Stanton RE (1972) J Am Chem Soc 94: 8618–8620
26. Metiu H, Ross J, Silbey R, George TF (1974) J Chem Phys 61: 3200–3209
27. Stanton RE, McIver JW (1975) J Am Chem Soc 97: 3632–3646
28. Pechukas P (1976) J Chem Phys 64: 1516–1521
29. Collard KG, Hall GG (1977) Int J Quantum Chem 12: 623–637
30. Nalewajski RF, Carlton TS (1978) Acta Phys Pol A 53: 321–338
31. Carpenter BK (1985) J Am Chem Soc 107: 5730–5732
32. Tachibana A, Okazaki I, Koizumi M, Hori K, Yamabe T (1985) J Am Chem Soc 107: 1190–1196
33. Tachibana A, Fueno H, Yamabe T (1986) J Am Chem Soc 108: 4346–4352
34. Tachibana A, Fueno H, Okazaki I, Yamabe T (1992) Int J Quantum Chem 42: 929–930
35. Valtazanos P, Ruedenberg K (1986) Theor Chim Acta 69: 281–307
36. Kraus WA, DePristo AE (1986) Theor Chim Acta 69: 309–322
37. Basilevsky MV (1987) Theor Chim Acta 72: 63–67
38. Baker J, Gill PMW (1988) J Comput Chem 9: 465–475
39. Kurosaki Y, Takayanagi T (2000) J Mol Struct (THEOCHEM) 507: 119–126
40. Malone S, Hegarty AF, Nguyen MT (1988) J Chem Soc Perkin Trans II 477–483
41. Frey RF, Davidson ER (1988) J Chem Phys 88: 1775–1785
42. Koseki S, Gordon MS (1989) J Phys Chem 93: 118–125
43. Bosch E, Moreno M, Lluch JM, Bertran J (1989) Chem Phys Lett 160: 543–548
44. Minyaev RM, Kletskii ME (1989) J Struct Chim 30: 202–210, (in Russian 40–48)
45. Minyaev RM (1991) J Struct Chim 32: 559–589, (in Russian 127–154)
46. Minyaev RM (1993) J Struct Chim 34: 829–843, (in Russian 3–19)
47. Minyaev RM (1994) Russian Chem Rev 63: 883–903, (in Russian 939–961)
48. Minyaev RM, Wales DJ (1994) J Chem Soc Faraday Trans 90: 1831–1837
49. Minyaev RM, Wales DJ (1994) J Chem Soc Faraday Trans 90: 1839–1847
50. Minyaev RM, Wales DJ (1994) Chem Phys Lett 218: 413–421
51. Minyaev RM (1994) Int J Quantum Chem 49: 105–127
52. Minyaev RM (1995) Zh Fiz Khim 69: 408–415 (in Russian)
53. Minyaev RM, Lepin EA (1997) Mendeleev Commun 189–190
54. Minyaev RM (1998) Russ Chem Bull 47: 8–16
55. Smith BJ, Swanton DJ, Pople JA, Schaefer HF, Radom L (1990) J Chem Phys 92: 1240–1247
56. Marcus RA (1991) J Phys Chem 95: 8236–8243
57. Shida N, Barbara PF, Almlöf J (1991) J Chem Phys 94: 3633–3643
58. Windus TL, Gordon MS, Burggraf LW, Davis LP (1991) J Am Chem Soc 113: 4356–4357
59. Windus TL, Gordon MS (1992) Theor Chim Acta 83: 21–30
60. Bone RGA, Rowlands TW, Handy NC, Stone AJ (1991) Mol Phys 72: 33–73
61. Bone RGA (1993) Chem Phys 178: 255–277
62. Stanton JF, Gauss J, Bartlett RJ, Helgaker T, Jørgensen P, Jensen HJA, Taylor PR (1992) J Chem Phys 97: 1211–1216
63. Hrovat DA, Bordon WT (1992) J Am Chem Soc 114: 5879–5881
64. Vager Z, Graber T, Kanter EP, Zajfman D (1993) Phys Rev Lett 70: 3549–3552
65. Manolopoulos DE, Stark K, Werner HJ, Arnold DN, Badfort SE, Neumark DM (1993) Science 262: 1852–1855
66. Lyons BA, Pfeifer J, Peterson TH, Carpenter BK (1993) J Am Chem Soc 115: 2427–2437
67. Yamamoto N, Bernardi F, Bottoni A, Olivucci M, Robb MA, Wilsey S (1994) J Am Chem Soc 116: 2064–2074
68. Ischtwan J, Collins MA (1994) J Chem Phys 100: 8080–8088
69. Taketsugu T, Hirano T (1993) J Chem Phys 99: 9806–9814
70. Taketsugu T, Hirano T (1994) J Mol Struct (THEOCHEM) 130: 169–176
71. Taketsugu T, Gordon MS (1995) J Chem Phys 103: 10042–10049
72. Taketsugu T, Tajima N, Hirao K (1996) J Chem Phys 105: 1933–1939
73. Yanai Y, Taketsugu T, Hirano T (1997) J Chem Phys 107: 1137–1146
74. Taketsugu T, Yanai Y, Hirao K, Gordon MS (1998) J Mol Struct (THEOCHEM) 451: 163–177
75. Takata T, Taketsugu T, Hirao K, Gordon MS (1998) J Chem Phys 109: 4281–4289
76. Kumeda Y, Taketsugu T (2000) J Chem Phys 113: 477–484
77. Taketsugu T, Kumeda Y (2001) J Chem Phys 114: 6973–6982
78. Simons J (1993) Int J Quantum Chem 48: 211–218
79. Schlegel HB (1994) J Chem Soc Faraday Trans 90: 1569–1574
80. Schlegel HB (1998) In: Schleyer PvR (ed) Encyclopedia of computational chemistry. Wiley, New York, pp 2432–2437
81. Quapp W (1994) J Chem Soc Faraday Trans 90: 1607–1609
82. Okada K, Sugimoto M, Saito K (1994) Chem Phys 189: 629–636
83. Tomimoto M, Gō N (1995) J Phys Chem 99: 563–577
84. Liao JL, Wang HL, Xin HW (1995) Chin Sci Bull 40: 566–570
85. Paz JJ, Moreno M, Lluch JM (1995) J Chem Phys 103: 353–359
86. Chu CH, Ho JJ (1995) J Am Chem Soc 117: 1076–1082
87. Kapp J, Schreiner PR, Schleyer PvR (1996) J Am Chem Soc 118: 12154–12158

88. Garavelli M, Celani P, Bernardi F, Robb MA, Olivucci M (1997) J Am Chem Soc 119: 6891–6901
89. Shaik S, Danovich D, Sastry GN, Ayala PY, Schlegel HB (1997) J Am Chem Soc 119: 9237–9245
90. Ayala PY, Schlegel HB (1997) J Chem Phys 107: 375–384
91. Ayala PY, Schlegel HB (1998) J Chem Phys 108: 7560–7567
92. Schaad LJ, Hu J (1998) J Am Chem Soc 120: 1571–1580
93. Suresh CH, Gadre SR, Gejji SP (1998) Theor Chem Acc 99: 151–157
94. Shustov GV, Rauk A (1998) J Org Chem 63: 5413–5422
95. Pidun U, Frenking G (1998) Chem Eur J 4: 522–540.
96. Valdés H, Raýon VM, Sordo JA (1999) Chem Phys Lett 309: 265–273
97. Braña P, Menéndez B, Fernández T, Sordo JA (2000) J Phys Chem A 104: 10842–10854
98. Bian W, Werner HJ (2000) J Chem Phys 112: 220–229
99. Sakai S (2000) J Phys Chem A 104: 922–927
100. Bally T, Bernhard S, Matzinger S, Truttmann L, Zhu ZD, Roulin J-L, Marcinek A, Gebicki J, Williams F, Chen G-F, Roth HD, Herbertz T (2000) Chem Eur J 6: 849–857
101. Sanchez-Galvez A, Hunt P, Robb MA, Olivucci M, Vreven T, Schlegel HB (2000) J Am Chem Soc 122: 2911–2924
102. Kliesch W (2000) J Math Chem 28: 113–138
103. Choi TH, Park ST, Kim MS (2001) J Chem Phys 114: 6051–6057
104. Bartsch RA, Chae YM, Ham S, Birney DM (2001) J Am Chem Soc 123: 7479–7486
105. Gonzáles M, Valero R, Sayós R (2001) Chem Phys Lett 343: 119–129
106. Valdés H, Sordo JA (2001) Chem Phys Lett 333: 169–180
107. Mann DJ, Hase WL (2002) J Am Chem Soc 124: 3208–3209
108. Caramella P, Quadrelli P, Toma L (2002) J Am Chem Soc 124: 1130–1131
109. Quadrelli P, Romano S, Toma L, Caramella P (2002) Tetrahedron Lett 43: 8785–8789
110. Reyes MB, Lobkovsky EB, Carpenter BK (2002) J Am Chem Soc 124: 641–651
111. Debbert SL, Carpenter BK, Hrovat DA, Bordon WT (2002) J Am Chem Soc 124: 7896–7897
112. Yamataka H, Aida M, Dupuis M (2002) Chem Phys Lett 353: 310–316
113. Varandas AJC, Llanio-Trujillo JL (2002) Chem Phys Lett 356: 585–594
114. Castaño O, Palmeiro R, Frutos LM, Andrés JL (2002) J Comput Chem 23: 732–736
115. Joyeux M, Farantos SC, Schinke R (2002) J Phys Chem A 106: 5405–5421
116. Sako T, Yamanouchi K, Iachello F (2002) J Chem Phys 117: 1641–1649
117. Svitak JF, Tyng V, Kellman ME (2002) J Phys Chem A 106: 10797–10805
118. Singleton DA, Hang C, Szymanski MJ, Greenwald EE (2003) J Am Chem Soc 125: 1176–1177
119. Quapp W (2003) J Theor Comput Chem 2: 385–410
120. Lasorne B, Dive G, Lauvergnat D, Desouter-Lecomte M (2003) J Chem Phys 118: 5831–5840
121. Hirsch M, Quapp W, Heidrich D (1999) Phys Chem Chem Phys 1: 5291–5299
122. Quapp W, Melnikov V (2001) Phys Chem Chem Phys 3: 2735–2741
123. Quapp W, Heidrich D (2002) J Mol Struct (THEOCHEM) 585: 105–117
124. Fukui K (1970) J Phys Chem 74: 4161–4163
125. Tachibana A, Fukui K (1978) Theor Chim Acta 49: 321–347
126. Quapp W (2003) Optimization 52: 317–331
127. Quapp W (2001) J Comput Chem 22: 537–540
128. Hirsch M, Quapp W (2002) J Comput Chem 23: 887–894
129. Branin Jr. FH (1972) IBM J Res Develop 16: 504–522
130. Miller W, Handy NC, Adams JE (1980) J Chem Phys 72: 99–112
131. Palmeiro R, Frutos LM, Castaño O (2002) Int J Quantum Chem 86: 422–425
132. Jensen F (1998) Theor Chem Acc 99: 295–300
133. Jensen F (1995) J Chem Phys 102: 6706–6718
134. Allgower EL, Georg K (1990) Numerical continuation methods—An Introduction, Springer, Berlin Heidelberg New York
135. Rowe DJ, Ryman A (1982) J Math Phys 23: 732–735
136. Müller K, Brown LD (1979) Theor Chim Acta 53: 75–93
137. Jørgensen P, Jensen HJA, Helgaker T (1988) Theor Chim Acta 73: 55–65
138. González J, Giménez X, Bofill JM (2002) J Chem Phys 116: 8713–8722